AGU PUBLICATIONS

Water Resources Research

RESEARCH ARTICLE
10.1002/2014WR015963

Key Points:
- Blending observed and estimated precipitation creates a more complete and accurate product
- Drought and flood management practices require accurate precipitation estimates
- Bayesian approaches provide more complete information and uncertainty

Supporting Information:
- Readme
- Figure 7
- Figure 8
- Figure 9
- Figure 10
- Figure 11
- Figure 12
- Figure 13

Correspondence to:
A. Verdin,
andrew.verdin@colorado.edu

Citation:
Verdin, A., B. Rajagopalan, W. Kleiber, and C. Funk (2015), A Bayesian kriging approach for blending satellite and ground precipitation observations, *Water Resour. Res.*, *51*, 908–921, doi:10.1002/2014WR015963.

Received 9 JUN 2014
Accepted 8 JAN 2015
Accepted article online 14 JAN 2015
Published online 11 FEB 2015

A Bayesian kriging approach for blending satellite and ground precipitation observations

Andrew Verdin[1], Balaji Rajagopalan[1,2], William Kleiber[3], and Chris Funk[4,5]

[1]Department of Civil, Environmental, and Architectural Engineering, University of Colorado, Boulder, Colorado, USA, [2]Cooperative Institute for Research in Environmental Sciences, University of Colorado, Boulder, Colorado, USA, [3]Department of Applied Mathematics, University of Colorado, Boulder, Colorado, USA, [4]U.S. Geological Survey, Earth Resources Observation and Science Center, Sioux Falls, South Dakota, USA, [5]Climate Hazards Group, Geography Department, University of California, Santa Barbara, California, USA

Abstract Drought and flood management practices require accurate estimates of precipitation. Gauge observations, however, are often sparse in regions with complicated terrain, clustered in valleys, and of poor quality. Consequently, the spatial extent of wet events is poorly represented. Satellite-derived precipitation data are an attractive alternative, though they tend to underestimate the magnitude of wet events due to their dependency on retrieval algorithms and the indirect relationship between satellite infrared observations and precipitation intensities. Here we offer a Bayesian kriging approach for blending precipitation gauge data and the Climate Hazards Group Infrared Precipitation satellite-derived precipitation estimates for Central America, Colombia, and Venezuela. First, the gauge observations are modeled as a linear function of satellite-derived estimates and any number of other variables—for this research we include elevation. Prior distributions are defined for all model parameters and the posterior distributions are obtained simultaneously via Markov chain Monte Carlo sampling. The posterior distributions of these parameters are required for spatial estimation, and thus are obtained prior to implementing the spatial kriging model. This functional framework is applied to model parameters obtained by sampling from the posterior distributions, and the residuals of the linear model are subject to a spatial kriging model. Consequently, the posterior distributions and uncertainties of the blended precipitation estimates are obtained. We demonstrate this method by applying it to pentadal and monthly total precipitation fields during 2009. The model's performance and its inherent ability to capture wet events are investigated. We show that this blending method significantly improves upon the satellite-derived estimates and is also competitive in its ability to represent wet events. This procedure also provides a means to estimate a full conditional distribution of the "true" observed precipitation value at each grid cell.

1. Introduction

Drought and flood management practices require accurate estimates of precipitation in space and time. However, rain gauge observations are often sparse in regions with complex terrain, clustered in valleys or populated regions, and of poor temporal consistency. In these situations, gauge data may provide little information about the spatial extent and intensity of a given precipitation event. Due to its extensive spatial coverage, satellite-based rainfall estimates are an attractive and widely used alternative in such regions. Scientists have long used the relationships between satellite-observed infrared brightness temperatures, microwave radiation, outgoing longwave radiation, and precipitation intensities to estimate gridded precipitation values [*Arkin and Ardanuy*, 1989; *Adler et al*., 1994; *Kummerow et al*., 1998; *Sorooshian et al*., 2000; *Kidd et al*., 2003; *Joyce et al*., 2004; *Huffman et al*., 2007]. However, these estimates provide areal averages, and in complex terrain they tend to underestimate the intensity of wet events [*AghaKouchak et al*., 2011]. Other issues with satellite-based precipitation estimates include their dependency on any number of retrieval algorithms and the indirect relationship between satellite infrared radiation observations and precipitation intensities [*Xie and Arkin*, 1997]. Using unadjusted satellite-based precipitation estimates in hydrologic applications can lead to unreliable assessments of risk and reliability [*AghaKouchak et al*., 2011].

Over the years, there have been numerous studies focused on producing more accurate precipitation estimates. To address the inherent bias of satellite-based precipitation estimates, many of these approaches

implement unique methodologies for blending multiple data sources, typically rain gauge observations, radar data, satellite-based precipitation estimates, and numerical model output [*Xie and Arkin*, 1997; *Joyce and Arkin*, 1997; *Huffman et al*., 1995, 1997, 2001; *Xie et al*., 2003; *Adler et al*., 2003; *Vila et al*., 2009; *Rozante et al*., 2010; *Xie and Xiong*, 2011; *Lin and Wang*, 2011; *Berndt et al*., 2013; *Jin et al*., 2014].

One of the first widely available analyses, the Climate Prediction Center Merged Analysis of Precipitation (CMAP) [*Xie and Arkin*, 1997] was produced by blending a number of satellite-based estimates with rain gauge analyses and numerical model output. At its inception, CMAP provided a 17-year time series of global monthly analyses at 2.5° × 2.5° spatial resolution. The Global Precipitation Climatology Project (GPCP) has offered a suite of products over the years, produced by blending rain gauge analyses with a number of satellite-based estimates. Through the years, the GPCP has produced and improved these analyses [e.g., *Joyce and Arkin*, 1997; *Huffman et al*., 1995, 1997], which boast increasingly fine temporal ranges (monthly, pentadal (5 day), daily), spatial resolutions (2.5° × 2.5°, 2.5° × 2.5°, 1.0° × 1.0°, respectively), and unbounded global scales [*Adler et al*., 2003; *Xie et al*., 2003; *Huffman et al*., 2001].

Xie and Xiong [2011] offer a unique blending approach by matching the probability density functions of satellite-based estimates with those of rain gauge analyses in order to correct for bias. These bias-corrected satellite estimates are then blended with rain gauge analyses to produce robust, high-resolution analyses of precipitation. *Lin and Wang* [2011] adopt the model form of *Le and Zidek* [2006, chap. 10] to offer yet another approach to blending multiple bias-corrected satellite precipitation estimates, quantifying and removing the bias by comparing the estimates to the rain gauge observations within the respective pixels. A weighting technique based on rain gauge density is used to obtain final blended estimates.

A multiscale recursive estimation algorithm [*Chou et al*., 1994] for fusing precipitation data at distinctly different scales was performed and validated by *Gorenburg et al*. [2001]. Bayesian techniques were employed to condition precipitation estimates on direct measurements. Validation was carried out on data from the TOGA-COARE experiment, effectively fusing satellite microwave and shipborne radar data. This method is very effective in handling large data sets, as the hierarchical structure of the algorithm does not require calculation of large covariance matrices. *Tustison et al*. [2002] provides an assessment of the multiscale recursive estimation algorithm with application to Quantitative Precipitation Forecast verification. Specifically, sensitivities to model misspecification are analyzed. They concluded that misspecification of the model structure has much more significant effect on estimation than a misspecification of the model parameters of a correctly specified model structure. Although the assessment was carried out only on QPF verification, it follows that model definition sensitivities are pertinent to a variety of applications.

Sinclair and Pegram [2005] employ the methodology developed by *Ehret* [2003] known as Conditional Merging to blend rain gauge data with radar-based rainfall estimates. In this technique, the mean field of the rain gauges is maintained via ordinary kriging, while the bias of the interpolated values is reduced by incorporating the spatial structure as reported by radar. Although used in an artificial experiment, this method proved very effective in reducing variance and bias of error estimates. *Bárdossy and Pegram* [2013] provide two new methodologies for interpolating precipitation data from daily to yearly accumulation scales. Gaussian copulas and unsymmetrical v-copulas, both incorporating elevation as an exogenous variable, were developed and validated in a large region of Germany. For this study region, both copula-based methods improve on traditional methods such as ordinary kriging and kriging with external drift while providing robust conditional distributions at all target points. *Berndt et al*. [2013] provide a comparison of different blending techniques—kriging and indicator kriging, both with external drift, and conditional merging—for blending rain gauge and radar data at a wide variety of temporal resolutions (from 10 min to 6 h). They also investigate the impact of station density on the blending performance. Even when the correlation between radar pixels and the corresponding rain gauge values was weak, they found the blending process benefitted from this additional information.

Specific to this research, recent South American rainfall estimation work has focused on improving real-time satellite-based precipitation estimates using robust bias correction measures. *Vila et al*. [2009] developed a stepwise method for blending daily Tropical Rainfall Measuring Mission (TRMM) Multisatellite Precipitation Analysis (TMPA) [*Huffman et al*., 2007] version 3B42RT output with rain gauge data for South America. The blended analysis is a weighted combination of two distinct bias-correction schemes that also minimize error. *Rozante et al*. [2010] provide a blending technique that uses the Barnes objective analysis

method to interpolate and blend TRMM satellite estimates with rain gauge data. This algorithm provides a quick and efficient technique for blending satellite and surface observations, specifically in regions with sparsely distributed gauge observations.

Incorporating a Bayesian framework to blend data sets of distinctly different spatial scales—as proposed in this research—is not a new concept. *Sansó and Guenni* [1999] developed a Bayesian space-time model to predict monthly rainfall amounts for 80 stations in the Venezuelan state of Guárico. A Markov chain Monte Carlo framework was adopted for the handling of missing data and dry spells. By using the predictive density of the data, the model can also estimate the probability of a dry period. Natural rainfall magnitudes and space-time variability are reproduced with good skill.

Two other Bayesian approaches to blending data sets via "Bayesian melding" are *Fuentes and Raftery* [2005] and *Berrocal et al*. [2010]. While these studies focus on air quality data as opposed to precipitation totals, the methodology is assumed portable to any number of different data sets. *Fuentes and Raftery* [2005] implement a full Bayesian spatiotemporal model to produce maps of dry deposition air pollution levels and the uncertainty about them. The two data sources used are point-level observations (air quality readings from 50 monitoring stations) and gridded numerical model output. Due to the numerical model's tendency to perform poorly in regions surrounding power plants, this method has proven to be worthwhile for improving numerical model output. Similarly, *Berrocal et al*. [2010] offer a Bayesian model-based methodology for blending the same class of data sources. While the paper explicitly examines a bivariate space-time downscaler, the potential for a multivariate downscaler is evident, which is especially impressive. Spatial downscaling is an increasingly important practice, considering that gridded numerical model output represents areal averages of a relatively large geographical region, which can lead to spatial misalignment when comparing data sets.

One of the most recent advancements in this field is a Bayesian spatiotemporal model-based approach to blending satellite-based estimates with rain gauge observations [*Jin et al*., 2014]. As in *Lin and Wang* [2011], they adopted the model form as investigated in *Le and Zidek* [2006, chap. 10] for application in a southwestern region of Canada. They show that their method improved upon *Lin and Wang* [2011] in small training data sets—thus, it is useful for blending networks of sparse gauge measurements, as is commonly the case in Canada. One limitation to the original methodology of *Jin et al*. [2014] had been a requirement that the number of time steps exceeds the number of spatial locations. However, they have developed a working solution to this problem, and the results are promising.

Bayesian kriging (hereafter BK) [see *Banerjee et al*., 2004] is a powerful approach to kriging that treats the covariance structure as unknown. Instead of using traditional methods of parameter estimation such as ordinary least squares or maximum likelihood, a set of prior distributions for parameters and hyperparameters is defined and routinely updated, based on available data, via Markov chain Monte Carlo (MCMC) simulation. This in turn produces a posterior distribution for each of the parameters, which effectively quantifies parameter uncertainty, a problem that has plagued traditional methods for decades. Over the years, BK has been applied for a variety of purposes, namely to attain not only a spatial structure but also the uncertainty of geophysical and ecological processes, environmental contamination fields, topography, and subsurface processes and characteristics, among others [*Omre*, 1987; *Handcock and Stein*, 1993; *Cui et al*., 1995; *Chen and Hubbard*, 2001; *Aelion et al*., 2009; *Le and Zidek*, 1992; *Sahu and Mardia*, 2005].

In this research, the authors propose a BK approach to blending in situ rain gauge observations with satellite-based estimates, with application in Central America, Colombia, and Venezuela. This methodology expands on the work of *Verdin* [2013, chap. 2] which is a spatial interpolation model-based blending comparison study. The skill of two models—residual kriging (RK) and *k*-nearest neighbor local polynomial—was explored. While both models substantially improved the satellite-based estimates, there were certain shortcomings that are addressed in this manuscript. For example, when predicting on the satellite grid, the RK model tends to estimate the expected value of the process. Because of this, in data-sparse regions, the blended products resulting from the RK blending method are similar in magnitude and spatial structure to the satellite-derived estimates, which are biased in regions with complex topography. Conversely, the local polynomial model uses local functional estimation, which is powerful in capturing the local nonlinearities of precipitation very well. In data-sparse regions, however, the local polynomial model is susceptible to extrapolation error, resulting in great, unwarranted changes from the satellite-derived estimates. It is believed that

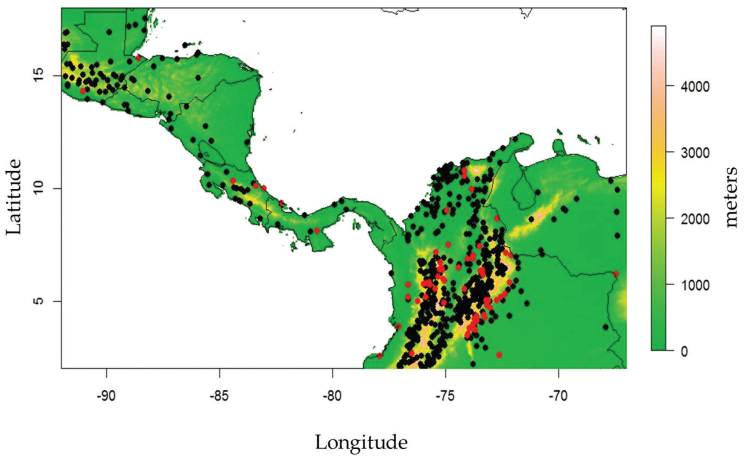

Figure 1. Study region geography, *z* scale is elevation. Gauge locations shown in black; locations of wet events for July 2009 are in red (see section 4.4).

implementing a Bayesian framework for a model-based approach is straightforward and simple enough to be applied for any study region of comparable climatology and topography, while being powerful enough to address the shortcomings of traditional model-based blending methods addressed above. For this reason, in section 4 of this manuscript we compare the BK and RK models side-by-side. Data-sparse regions will see warranted corrections when necessary, based on the model parameters' posterior distributions. Applying a Bayesian framework to a simple linear model will simplify the blending process, specifically by maintaining the mean function and correcting for local nonlinearities by incorporating elevation as a covariate and implementing a zero-mean Gaussian error field with covariance defined by the residuals. Here, we show that using BK over Central and South America not only produces accurate low-bias combinations of satellite precipitation and gauge observations, but also provides a means to estimate a full conditional distribution of the "true" total precipitation value for each grid cell—information that will greatly improve the quantification of estimation uncertainty at each grid cell. It follows that these BK results are a valuable contribution to hydrologic early warning and modeling systems, supporting ensemble-based assessments of possible risks and impacts.

The study region and data are described in section 2, followed by an in-depth description of the BK framework in section 3. An overview and analysis of the results is included in section 4, and conclusions and future work in the last section.

2. Study Region and Data

2.1. Study Region

This research focuses on a Central and South American region, specifically Guatemala, Belize, El Salvador, Honduras, Nicaragua, Costa Rica, Panama, Colombia, and Venezuela (see Figure 1). The dry season in the region extends from December to early May and the effects of both Pacific and Atlantic tropical depressions are felt during the wet season that extends from mid-May to November. A major contributor to the prolonged wet season is the intertropical convergence zone (ITCZ)—an asymmetric band of convection that encircles the globe. The position of the ITCZ is nonstationary due to the seasonal shift of the trade winds.

Another cause for intense spatial variability of rainfall within the study region is its complex geography. Elevation in this area ranges from sea level to nearly 5000 m (as can be seen in Figure 1) with numerous mountain ranges spanning Central America, Venezuela, and Colombia. Costa Rica and Guatemala have steep elevation gradients, making them vulnerable to extreme weather spawning from both Pacific and Atlantic tropical depressions. Tropical mountain ranges cause an abrupt rising of warm, wet air. As this air rises, it cools rather quickly, releasing moisture from the air as precipitation. This is known as orographic precipitation and is a major contributor to the variability in extreme precipitation events in the region.

Given the spatial and temporal variability of rainfall in this region, coupled with vulnerable socioeconomic conditions, droughts and floods can have a debilitating impact on countries in this region. It has been observed that a single wet event may result in flooding, landslides, and potentially millions of dollars in damages, thus setting the national infrastructure back many years. Conversely, a prolonged dry spell may be equally devastating, causing widespread crop failures that can reduce food availability and agricultural

incomes. Thus, a comprehensive understanding of rainfall variability is of critical importance for resources planning and management.

2.2. Data

Two precipitation data sets are utilized in this research—gauge measurements and satellite-derived estimates. Rain gauge measurements are point values that tend to be clustered in populous and low elevation areas and sparsely scattered throughout the domain; the satellite-based products are high-resolution areal average rainfall estimates. The gauge data used in this research (shown in Figure 1) were collected from the Global Historical Climatology Network (GHCN) [*Lawrimore et al.*, 2011], as well as partner sources of the University of California, Santa Barbara, Climate Hazards Group (CHG); quality control and pentadal-aggregation techniques of the partner source data were implemented by the CHG to produce station data of the same temporal scale as the available CHG Infrared Precipitation (CHIRP) products [*Funk et al.*, 2014], a fine-resolution ($0.05^\circ \times 0.05^\circ$) pentadal product with temporal range from the first pentad of January 1981 through the near present. There are six pentads per month, regardless of month length. For example, the sixth pentad of October will consistently be the sum of the last 6 days, 26–31 October. The sixth pentad of February, however, will be the sum of either 3 or 4 days, depending on leap year status. Monthly precipitation totals are obtained by summing the six pentads of any given month.

3. Bayesian Kriging

Before describing the blending method developed in this research, we introduce some notation. Let $Y_{sat}(s)$ and $Y_{obs}(s)$ be the satellite estimates and observed precipitation at location s, respectively. As the observation network is likely irregularly spaced, each observation within the network is assigned to its nearest grid cell. Due to the fine resolution of the satellite estimates, it is fair to assume the observation is representative of the areal average precipitation total within the grid it is assigned. Suppose the observation network has spatial locations s_i, $i=1, \ldots, N_t$, where N_t is the number of stations with nonmissing data for time t. Easting and northing (from the Prime Meridian) are used as spatial information where $s \in \mathbb{R}^3$ includes easting, northing, and elevation. Define $X_1(s)$ and $X_2(s)$ to be covariates related to observed precipitation, where $X_1(s)=Y_{sat}(s)$ and $X_2(s)$ is the elevation at location s; any number of other covariates may be incorporated. To briefly describe the blending method developed in this research, the observation at location s_i and time t is assumed to be a realization of a unique Gaussian process, the mean of which is modeled as a linear function of covariates; the residual is modeled as a spatial process. The BK model involves an observation process that we decompose as

$$Y_{obs}(s)=\beta_1 X_1(s)+\beta_2 X_2(s)+Z(s) \tag{1}$$

The residual process $Z(s)$ is assumed to be a mean zero Gaussian process with exponential covariance function (see equation (2)) with marginal variance σ^2 and effective range ϕ which can be interpreted as the distance at which covariance decays to zero. We do not include a nugget effect τ^2 as exploratory analysis suggested no presence of one—a zero nugget also forces the kriging model to be an exact interpolator of points included in the fit.

$$\tilde{\gamma}(h)=\tau^2+\sigma^2\left[1-exp(-\frac{|h|}{\phi})\right] \tag{2}$$

This model structure treats rain gauge measurements as "perfect" information. However, data from both the GHCN and CHG partner sources have been subjected to a suite of quality assurance reviews such that this is not an unreasonable assumption. Similarly, an assumption of stationarity can be questionable over large spatial domains. However, the details of implementing and choosing a nonstationary modeling framework are beyond the scope of this research (these will be addressed in section 5).

A Bayesian approach involves prior distributions on the model parameters. The linear model has two β coefficients, which we assign flat priors [*Finley et al.*, 2009]. We endow σ^2 with an inverse Gamma prior with shape $\alpha = 5$ and scale $\beta=1/100$. Finally, ϕ is given a uniform prior over a physically meaningful set of values. The range of the uniform is obtained as follows: a linear model is fit to the data of the form $Y_{obs}(s)=\beta_1 X_1(s)+\beta_2 X_2(s)+Z(s)$ using ordinary least squares to estimate the coefficients. An exponential variogram is

fitted to the empirical isotropic variogram based on observed residuals $Z(s)$. The empirical variogram is defined as

$$\gamma(h)=\frac{1}{2}Var[Z(s_i)-Z(s_j)] \tag{3}$$

where $h=||s_i-s_j||$ is the Euclidean distance between observation locations s_i and s_j. The effective range (ϕ) of this empirical variogram is used as a midpoint for the uniform prior distribution defined above, with upper and lower bounds defined as $+75\%$ and -75% of the midpoint value—e.g., with lower bound 0.25ϕ and upper bound 1.75ϕ. The range parameter theoretically has a finite range and this approach provides a wide yet realistic region. Restricting the prior range in an ad hoc manner such as this is necessary for the spatial parameters since they are inconsistently estimable under infill asymptotics [*Zhang*, 2004]. Fortunately, even though the pair of variance and range are not consistently estimable, a quantity that involves both is consistently estimable, and it is this quantity that is important for spatial prediction. We then define θ as a vector of all model parameters,

$$\theta=\{\beta_1,\beta_2,\sigma^2,\phi\} \tag{4}$$

The parameters are estimated in a Bayesian framework, wherein we seek the posterior distribution of θ—e.g., the conditional distribution of θ given the data, $p(\theta|Y_{obs})$—which can be expressed using Bayes' rule as follows:

$$p(\theta|Y_{obs})=\frac{p(Y_{obs}|\theta)p(\theta)}{p(Y_{obs})}\propto p(Y_{obs}|\theta)p(\theta) \tag{5}$$

where $p(Y_{obs}|\theta)$ is the likelihood function for the observed data given the parameters and $p(\theta)$ is the prior joint distribution of the parameters. Assuming independence of the prior distributions of the parameters, the prior joint distribution of parameters factors into the product of the prior distributions, and the posterior density simplifies to

$$p(\theta|Y_{obs})\propto p(Y_{obs}|\theta)\prod_i p(\theta_i) \tag{6}$$

The posterior distributions of the parameters are obtained using MCMC simulations [*Gallagher et al.*, 2009], the standard method for parameter estimation in a Bayesian framework. The MCMC routine samples parameter values from their respective prior distributions, which are accepted (or rejected) using the traditional Metropolis ratio [*Metropolis et al.*, 1953]. To obtain robust posterior distributions of these parameters, 15,000 MCMC simulations are carried out, thus yielding 15,000 values of θ. However, due to a necessary burn-in time, the first 5,000 values are discarded, leaving us with 10,000 posterior samples [*Finley et al.*, 2009]. To ensure convergence, trace plots for all model parameters were visually inspected and verified.

In some statistical applications, the posterior distributions of the model parameters are of primary interest. However, for our blending purposes, we seek the posterior predictive distribution of the process.

$$f(Y_{obs}(s'_i)|Y_{obs})=\int f(Y_{obs}(s'_i),\theta|Y_{obs})d\theta \tag{7}$$

Specifically, at a new set of spatial locations $s'_i, i=1,\ldots,n$, we seek the conditional distribution $p(Y_{obs}(s'_1),\ldots,Y_{obs}(s'_n),\theta|Y_{obs})$. Samples from this posterior predictive distribution can be readily generated based on the MCMC posterior samples. To sample from this distribution, we first sample from the posterior of θ, followed by a sample from the conditional distribution of $Y_{obs}(s'_i)|Y_{obs}$. Repeating this procedure numerous times provides samples from the posterior predictive distribution. In particular, with the posterior predictive samples of the rainfall process at each grid point, it is possible to create spatial maps of the mean, median, and confidence intervals (e.g., 5^{th} and 95^{th} percentiles) of predicted rainfall.

In this research, the "spBayes" library [*Finley and Banerjee*, 2013] in R [*R Development Core Team*, 2011] is used for model fitting, as it is capable of fitting multivariate spatiotemporal models using MCMC simulation. The spatial estimation process, via ordinary kriging, is carried out in R as well, utilizing the "fields" library [*Furrer et al.*, 2012].

4. Results

Analysis of the results is divided into the following categories: model fitting, model validation, model predictions, and performance evaluation for wet events. Analysis was performed on several months but we

focus on monthly accumulations for January and July 2009—representative dry and wet months, respectively—as well as the fourth pentad of August (P4) 2009, as it is one of the wettest pentads of 2009 (yielding a maximum observation of 385 mm where the CHIRP reports only 130 mm). However, in the interest of space we show results for July and discuss the results for January and P4. Figures for January can be seen in *Verdin* [2013, chap. 3]; figures for P4 can be found in the supporting information of this manuscript.

4.1. Model Fitting

The prior and posterior distributions for the model parameters for July can be seen in Figure 2. Interpretation of these parameters can be suspect due to spatial confounding issues [*Paciorek*, 2010]. Posterior samples indicate substantially different parameter regions than the prior distributions, indicating Bayesian learning has occurred. Posterior convergence was assessed by visually inspecting trace plots (not shown). It should be noted that, although the prior distributions for the β parameters are assumed independent, the posterior distributions exhibit dependent tendencies. There is nonnegligible negative correlation between β_1 and β_2. It should also be noted that in Figure 2 the prior distributions for the β parameters appear to be zero, when in fact the flat priors have such wide ranges that, when compared to the nicely converged posterior distributions of the β parameters, they only appear to be zero. The posterior distribution for ϕ is imperfect due to a well-documented problem with identifying σ^2 and ϕ simultaneously. Even though the spatial variance and range parameter are inconsistently estimable within an infill asymptotics framework, for the purposes of spatial prediction, optimal predictions can still be made [*Zhang*, 2004]. Results are consistent from monthly to pentadal temporal scales, with only a change in magnitude for the kriging parameters σ and ϕ. Figure 3a shows the empirical and theoretical variograms based on median parameters of the posterior distributions shown in Figure 2. The theoretical variogram matches the empirical variogram closely—as is the case for January and P4—which indicates a good fit. Random samples from these posterior distributions were used to produce posterior predictive distributions of the models' estimates of precipitation at each observation location s_i. For each parameter, a random value from its respective posterior

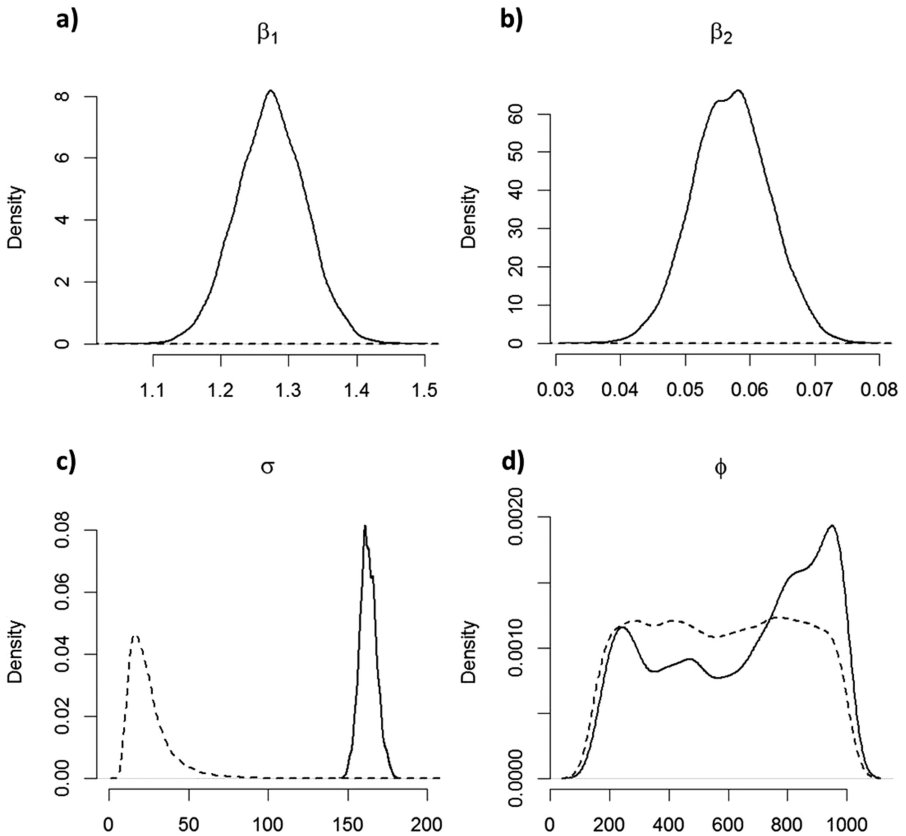

Figure 2. Prior (dashed lines) and posterior (solid lines) distributions for July 2009; (a and b) Regression coefficients and (c and d) kriging parameters.

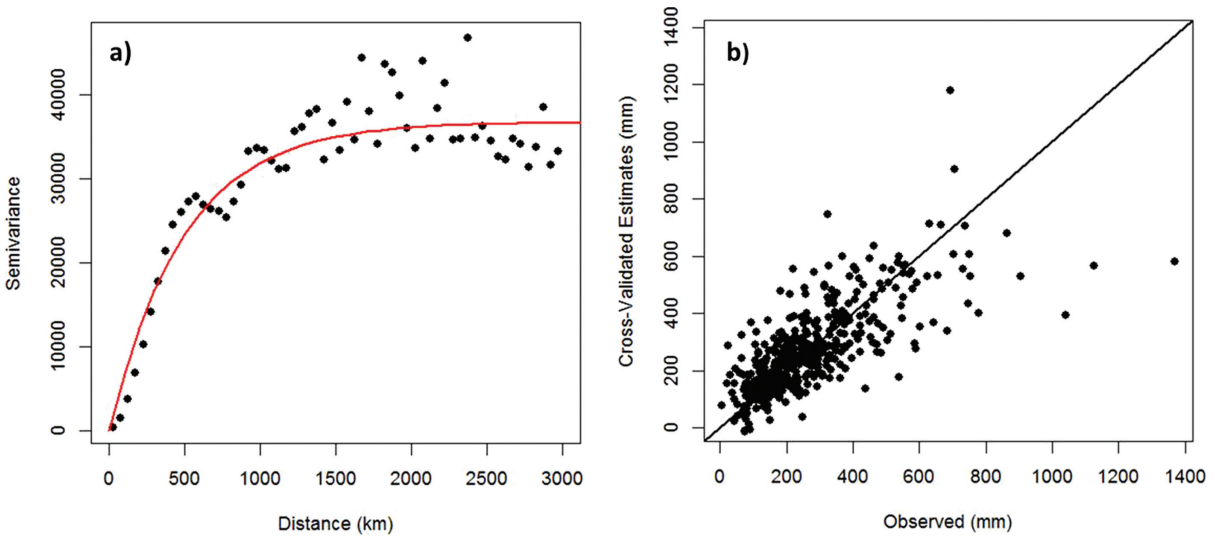

Figure 3. July 2009 precipitation—(a) empirical (black) and theoretical (red) variograms based on median parameters of the posterior distributions shown in Figure 2, (b) median leave-one-out cross-validation performance.

distribution is sampled. With the values of β_1 and β_2 we may reproduce the mean function; with kriging parameters σ and ϕ we may produce the corresponding residuals.

4.2. Model Validation

To test the out-of-sample predictability of the BK model, leave-one-out cross validation (LOOCV) was carried out 10,000 times to produce a full conditional distribution of predicted values. LOOCV is a validation procedure wherein one observation Y_{obs_i} and its covariates are dropped from the model fitting process and this model is used to estimate the dropped observation. Because the observation and its covariates were not included in the model, its estimate may be treated as a prediction. This process is repeated until all observations have been predicted, thus producing an ensemble of predictions that may be compared to the observations. Scatterplots are shown (Figure 3b) and summary statistics are calculated for the median of the full conditional distribution and are reported below. For a more robust comparison, a residual kriging (RK) model with easting, northing and elevation as covariates (as defined in *Verdin* [2013, chap. 2]) is also validated and discussed alongside the BK model and CHIRP. A nonparametric local polynomial method was compared alongside RK in *Verdin* [2013, chap. 2], and has been shown to be comparable in skill, thus will not be discussed. For a complete comparison of RK to local polynomial, see *Verdin* [2013, chap. 2]. Another more intense validation method was carried out by randomly dropping 25% of the observations, fitting the model on the remaining data, and predicting the dropped points. Three skill measures, root mean square error (RMSE; equation (8)), mean absolute error (MAE; equation (9)), and percent bias (% Bias; equation (10)) were computed, where N denotes the number of dropped observations. To quantify the variability of model skill, this was repeated 100 times—such that each iteration has an independent random sample of dropped observations—and the skill measures are shown as boxplots in Figure 4. For comparison, the skill measures of the CHIRP product are included as dots. To further stress the predictive capability of the model, the aforementioned validation technique was repeated with 50% of the observations being dropped. Figure 3b shows the median LOOCV results for July; Figure 4 shows the boxplots of skill measures from the drop-50% cross-validation procedure for July—drop-25% results can be seen in *Verdin* [2013, chap. 3]. Note the validation statistics are similar for all months and pentads in the test period.

$$RMSE = \sqrt{\frac{1}{N}\sum_{i=1}^{N}(\hat{Y}_{obs} - Y_{obs})^2} \tag{8}$$

$$MAE = \frac{1}{N}\sum_{i=1}^{N}|\hat{Y}_{obs} - Y_{obs}| \tag{9}$$

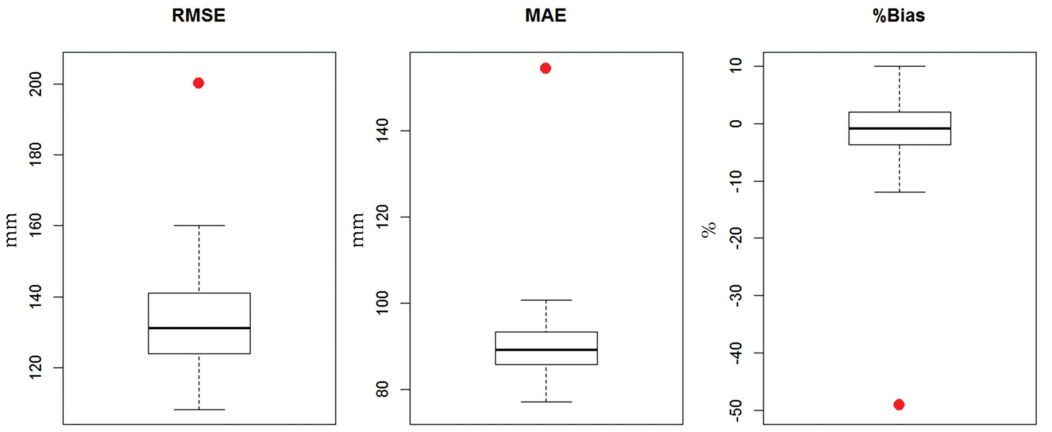

Figure 4. Drop-50% validation for July 2009 precipitation, (a) RMSE, (b) MAE, and (c) % Bias (CHIRP statistics shown as point).

$$\%Bias = 100\,\frac{\sum_{i=1}^{N}(\hat{Y}_{obs} - Y_{obs})}{\sum_{i=1}^{N} Y_{obs}} \tag{10}$$

For January—or any month where the CHIRP is a good estimator of precipitation totals—the LOOCV output proves the BK model is capable of reducing both bias and error of the CHIRP. RMSE for BK is 70 mm, RK is 76 mm, while that of the CHIRP is 76 mm. MAE is 45 mm for BK, 51 mm for RK, while CHIRP is 50 mm. The resulting bias from BK is only 0.3%, that from RK is 0%, while the CHIRP has inherent bias of −11.1%. Similarly, for July—or any month where the CHIRP fails in estimating precipitation totals—the LOOCV output of the BK model effectively eliminates bias and greatly reduces the inherent satellite errors. RMSE for BK is 118 mm, RK is 139 mm, while that of the CHIRP is 200 mm. MAE is 79 mm for BK, 99 mm for RK, while CHIRP is 154 mm. The resulting bias from BK is 0.0%, RK has a mere 0.4%, both of which have diminished greatly from −49%, the bias of the CHIRP product. For P4, the representative wet pentad, LOOCV produces results proving that the model eliminates bias and reduces error. For the BK model, RMSE is 38 mm, RK is 37 mm, while that of the CHIRP product is 40 mm. Similarly, MAE is 25 mm for both BK and RK, while that of the CHIRP product is 26 mm. The resulting bias from BK is only 0.1%, RK has 1% bias, and the CHIRP product has inherent bias of −21.4%.

Figure 4 reports the results of the drop-50% validation measure—proving that the BK model greatly reduces error and bias when compared to the CHIRP. Both RMSE and MAE were reduced by at least 30%, but the most striking result is the reduction in bias from −49% to nearly zero for both validation measures. The results from drop-25% are comparable to those shown in Figure 4. Similar results were obtained for other months (figures not shown). For the pentadal scale, the median values of RMSE and MAE from cross validation are similar in magnitude to the CHIRP, though there is a significant reduction in % Bias. The pentad considered is one of the wettest, thus when 25% and 50% of observations are dropped from the model-fitting process its predictive ability is compromised. Considering this, the performance of the blending method is very good.

4.3. Model Predictions From Blending

The fitted models were used to make blended predictions on the CHIRP grid. As mentioned above, 15,000 samples from the posterior distributions of the parameters are used to obtain 15,000 estimates of rainfall at each grid point—with the first 5,000 discarded as burn in. For point-level support, the median (or mean) of the 10,000 remaining estimates may be plotted on the CHIRP grid. Note that the posterior predictive sample distributions from the BK model are Gaussian, such that the medians and means are effectively equal (please see Figure 13 in the supporting information for a figure depicting the 95% uncertainty envelope with respect to the observed values). Similarly, a robust confidence interval (5^{th} and 95^{th} percentile) can be computed to visualize and quantify the range of uncertainty in the model's predictions. These gridded

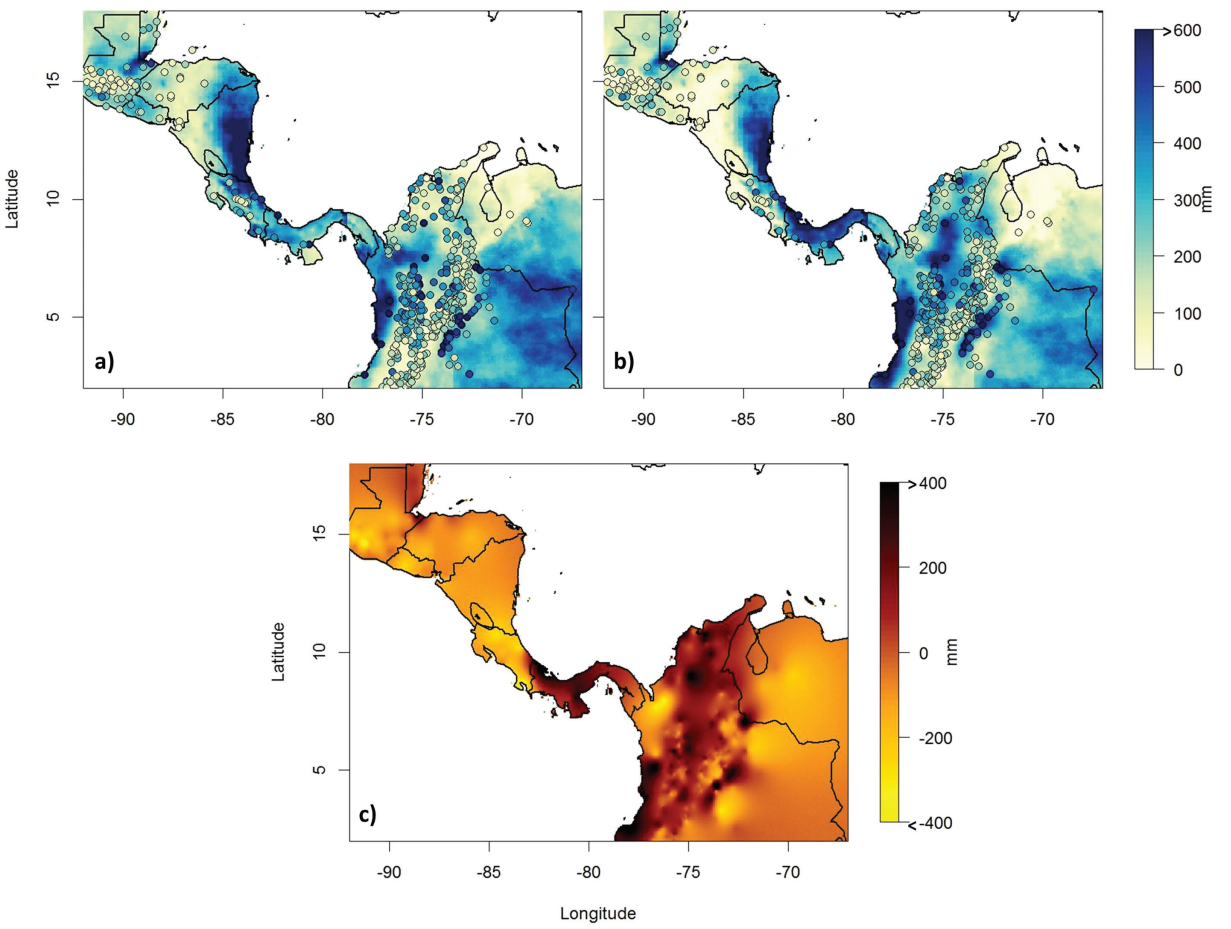

Figure 5. July 2009 precipitation—(a and b) CHIRP and Bayesian median predictive blended estimates, respectively; station values on same color scale, (c) difference between Bayesian median predictive blended estimates and CHIRP (e.g., positive values indicate increase from CHIRP).

products are shown in Figure 5 for July. For ease of visualization, "wet" values (defined as exceeding the 85th percentile of all gauge measurements for a given month) are plotted as the same deep blue color.

Figure 5c shows the difference between the median BK blended estimates and CHIRP, illustrating that the blended estimates are higher over Nicaragua and Colombia, consistent with topography. There are very few regions with blended estimates lower than the CHIRP values, confirming its wet season underestimation tendencies with respect to rain gauge measurements.

The spatial maps of 5th and 95th percentiles from the predictive posterior distributions (Figure 6) also show consistent behavior with elevation. The difference between the lower bound and upper bound of this confidence interval is nonnegligible. However, access to the full distribution is helpful for better informing decision makers of drought and flood risks. Regions with low probability of supporting agriculture, or high probability of extreme precipitation, can be identified. The kriging standard deviation is quantified and shown in Figure 6c, showing that the uncertainty is greatest at locations furthest from observation locations.

Median blended estimates improve upon the CHIRP similarly for January—the greatest change occurring along the Caribbean coast of Honduras and Nicaragua, where the CHIRP overestimates the magnitude of precipitation by at least 100 mm. The magnitude of change from the CHIRP due to blending is small and has spatial coherency. There are many localized events in Colombia, implying there is great variability of rainfall even in this representative dry month. Further, it is apparent that much of the change is due to the estimation of the residual, Z, since CHIRP is a largely unbiased estimator during this month. Robust confidence intervals show a very small range, implying that this model is consistent in its estimation process.

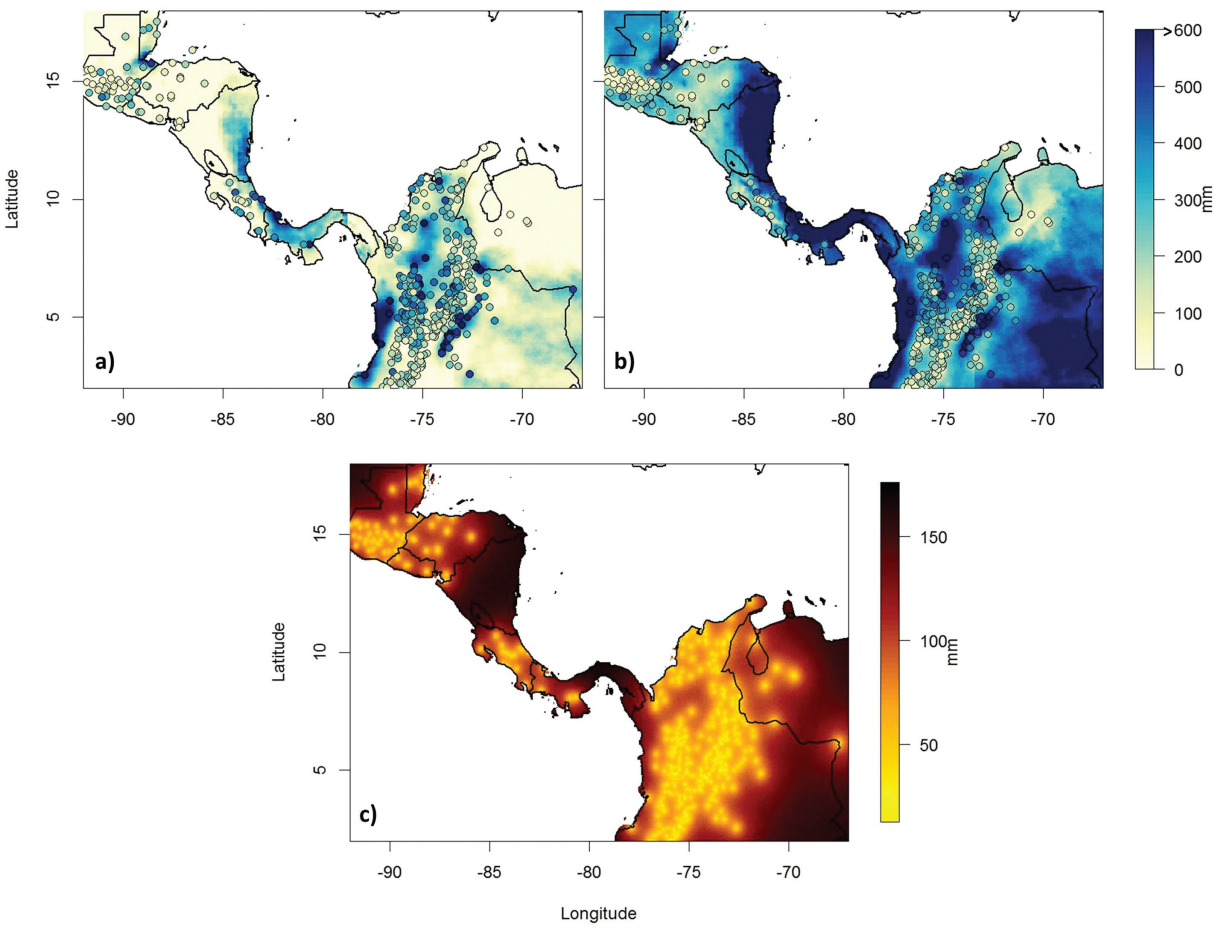

Figure 6. July 2009 precipitation—(a and b) 5th and 95th percentile of Bayesian predictive blended estimates, respectively; station values on same color scale, (c) kriging standard deviation from median parameters of the posterior distributions.

Similarly for P4, median blended estimates are higher over much of Nicaragua and Colombia, indicating the model has predicted more rain in these regions, which is corroborated by the observations. Similar to the monthly blended estimates, the regions of greatest increase for this pentad have a spatial pattern consistent with topography and the CHIRP estimate. Areas of increase and decrease are about equal, consistent with the tendency of the CHIRP to over and underestimate low and high-magnitude precipitation events, respectively, at the pentadal scale. The robust confidence interval of the posterior predictive samples is consistent from monthly to pentadal scale. The uncertainty in the kriging estimates is also similar in spatial structure, but smaller in magnitude when compared to monthly uncertainty.

4.4. Model Performance on Wet Events

Although the model presented in this research does not explicitly account for extremes, it is worthwhile to analyze its performance on wet events. As previously noted, satellite-derived precipitation estimates tend to underestimate wet events, thus biasing the risk and reliability analyses when used for hydrological modeling purposes. Good estimation of wet events is important for hydroclimatic hazard mitigation. The hazards associated with wet events consist of floods, landslides, and agricultural overland flow, all of which are destructive to a nation's infrastructure. We define a wet event at a location where monthly (pentadal) rainfall exceeds the 85th percentile of all rain gauge measurements for that month (pentad). For July, this quantity is 410 mm/month. The locations of these events and the majority of wet events occur in the mountainous and coastal regions (see Figure 1). Table 1 summarizes how blending with the BK model consistently improves the performance of the satellite estimate with respect to wet events. These statistics are

Table 1. Summary Statistics of Blending Performance on Wet Precipitation Events for July 2009

	RMSE (mm)	MAE (mm)	% Bias
Original CHIRP	386	344	−58.8%
Bayesian kriging	222	159	−19.2%
Residual kriging	322	279	−47.8%

computed from median LOOCV estimates. For a more robust comparison, statistics from the RK model are shown as well.

As can be seen in Table 1, the BK blending method has a strong positive impact on CHIRP performance with respect to wet precipitation events. Validation statistics indicate that blending reduces the error and inherent bias of the CHIRP satellite estimate. It should be noted that models for all months—as well as the pentadal model—in 2009 show similar skill with respect to wet events, thus it is worthwhile to implement this blending method on all available data to produce a more representative gridded time series of precipitation.

5. Summary and Conclusions

An approach for blending satellite-derived precipitation estimates with rain gauge measurements has been applied and validated with application in a Central and South American region. This blending method incorporates a Bayesian framework wherein precipitation at any location is assumed to be a realization of a Gaussian process, the mean estimates of which are modeled as a linear function of covariates (e.g., satellite-derived estimates and elevation). The residuals from this linear function are modeled as a spatial process using ordinary kriging. Prior distributions are defined and the posterior distributions of the model's parameters are obtained via MCMC, thus providing a complete representation of the variability and a quantification of the uncertainty in the parameters. The posterior distributions are used to produce predictive posterior distributions of precipitation, along with the respective probability density functions of precipitation estimates, at any arbitrary location.

The model was applied to January and July 2009 precipitation—dry and wet months, respectively—which showed very good model fits. As expected, the model is an exact fit at the observations due to the zero nugget. Leave-one-out, as well as drop-25% and drop-50%, cross-validation predictions of the model all showed good skill especially in eliminating all of the bias prevalent in satellite-derived estimates. Spatial estimates of blended precipitation showed robust and consistent improvements in that satellite estimates were enhanced appropriately based on the precipitation values of the surrounding gauges. The model was also tested with equally skillful performance on pentad time scales where the rainfall process is much more erratic and lacks spatial structure. The Bayesian kriging model proposed here has produced robust spatial precipitation maps, with full distributions at each grid cell, in near-real-time that will be of immense use in hydrologic and hazard models to provide risk estimates of various hazards in space, which can be used in mitigation efforts. Furthermore, this method offers a complementary suite to the standard methods based on kriging and less traditional *k*-nearest neighbor local polynomial [*Verdin*, 2013, chap. 2].

One of the major drawbacks of the blending method proposed here is the Gaussian assumption. Precipitation has positive support, thus a Gaussian assumption can result in negative estimates of precipitation in very dry regions. At coarse (i.e., monthly) temporal scales, however, this is rare. This Gaussian assumption is unique to each location s at every time t, and therefore is much more reasonable than to assume all residuals can be described by a single Gaussian distribution. It is not assumed all residuals at time t will be best described as Gaussian, rather each residual is uniquely Gaussian. Unfortunately, at finer temporal scales (i.e., daily) the Gaussian assumption is invalid. However, blended estimates of precipitation on pentadal time scales during wet seasons can provide insight into risk-prone regions of river basins, drive hydrologic models for modeling soil moisture, and help identify the potential for flooding and landslides.

The assumption of stationarity over a large spatial domain is another drawback of this blending method. However, the inclusion of elevation in the model structure does help to capture the nonstationarity in precipitation induced by elevation—which is a major contributor. The details of explicitly defining a nonstationary modeling framework are beyond the scope of this research. This manuscript is presented to provide a natural starting point for future research into this problem, which will address these apparent shortcomings.

Another relevant drawback of this method is that the satellite's gridded areal estimates are not downscaled for direct comparison to in situ measurements. However, the resolution of the satellite estimate is substantially fine (5 km × 5 km) that it is rare for multiple measurements to fall in the same grid cell. Still, there is

obvious misalignment in spatial scales, prompting the authors to consider a downscaling similar to *Berrocal et al*. [2010] in future work. Another shortcoming of this methodology is that it is applied separately for all available temporal snapshots—e.g., individual months or pentads. However, time series of precipitation (both satellite and gauge) are available, and incorporating the temporal variability can provide greater accuracy and reduce processing time for near-real-time application. This would involve fitting a separate generalized linear model for each gauged location using all the data available in time and fitting a spatial process for each model parameter. Thus, estimation of precipitation at any location would involve first obtaining the estimates of model parameters from the respective spatial process models and then combining in the hierarchy to obtain the precipitation estimates. The hierarchy could be non-Bayesian [*Verdin*, 2013, chap. 4], latent Gaussian process models [*Kleiber et al*., 2012], or a Bayesian approach used in other applications, particularly of modeling spatial extremes [*Cooley et al*., 2007; *Cooley and Sain*, 2010]. The use of temporal variability can help improve the near-real-time blended estimates by incorporating climate drivers that modulate the precipitation variability.

Acknowledgments
The authors thankfully acknowledge: three anonymous reviewers for their detailed and insightful reviews that improved this manuscript; NOAA Award NA11OAR4310151 for funding this research; and the Climate Hazards Group at the University of California, Santa Barbara, for the data and the support. Any use of trade, firm, or product names is for descriptive purposes only and does not imply endorsement by the U.S. Government.

References

Adler, R., et al. (2003), The Version-2 Global Precipitation Climatology Project (GPCP) monthly precipitation analysis (1979-Present), *J. Hydrometeorol.*, *4*, 1147–1167.

Adler, R. F., G. J. Huffman, and P. R. Keehn (1994), Global tropical rain estimates from microwave-adjusted geosynchoronous IR data, *Remote Sens. Rev.*, *11*, 125–152.

Aelion, C. M., H. T. Davis, Y. Liu, A. B. Lawson, and S. McDermott (2009), Validation of Bayesian kriging of arsenic, chromium, lead, and mercury surface soil concentrations based on internode sampling, *Environ. Sci. Technol.*, *43*(12), 4432–4438.

AghaKouchak, A., A. Behrangi, S. Sorooshian, K. Hsu, and E. Amitai (2011), Evaluation of satellite-retrieved extreme precipitation rates across the central United States, *J. Geophys. Res.*, *116*, D02115, doi:10.1029/2010JD014741.

Arkin, P., and P. Ardanuy (1989), Estimating climatic-scale precipitation from space: A review, *J. Clim.*, *2*, 1229–1238.

Banerjee, S., A. E. Gelfand, and B. P. Carlin (2004), *Hierarchical Modeling and Analysis for Spatial Data*, CRC Press, Boca Raton, Fla.

Bárdossy, A., and G. Pegram (2013), Interpolation of precipitation under topographic influence at different time scales, *Water Resour. Res.*, *49*, 4545–4565, doi:10.1002/wrcr.20307.

Berndt, C., E. Rabiei, and U. Haberlandt (2013), Geostatistical merging of rain gauge and radar data for high temporal resolutions and various station density scenarios, *J. Hydrol.*, *508*, 88–101, doi:10.1016/j.jhydrol.2013.10.028.

Berrocal, V., A. Gelfand, and D. Holland (2010), A bivariate space-time downscaler under space and time misalignment, *Ann. Appl. Stat.*, *4*(4), 1942–1975.

Chen, J., and S. Hubbard (2001), Estimating the hydraulic conductivity at the South Oyster Site from geophysical tomographic data using Bayesian techniques based on the normal linear regression model displays variation Oyster Site, *Water Resour. Res.*, *37*(6), 1603–1613.

Chou, K. C., A. S. Willsky, and A. Benveniste (1994), Multiscale recursive estimation, data fusion, and regularization, *IEEE Trans. Autom. Control*, *39*(3), 464–478.

Cooley, D., and S. R. Sain (2010), Spatial hierarchical modeling of precipitation extremes from a regional climate model, *J. Agric. Biol. Environ. Stat.*, *15*(3), 381–402, doi:10.1007/s13253-010-0023-9.

Cooley, D., D. Nychka, and P. Naveau (2007), Bayesian spatial modeling of extreme precipitation return levels, *J. Am. Stat. Assoc.*, *102*(479), 824–840, doi:10.1198/016214506000000780.

Cui, H., A. Stein, and D. O. N. E. Myers (1995), Extention of spatial information, Bayesian kriging and updating of prior variogram, *Environmetrics*, *6*, 373–384.

Ehret, U. (2003), Rainfall and flood nowcasting in small catchments using weather radar, PhD thesis, Eigenverlag des Inst. für Wasserbau an der Univ. Stuttgart, Stuttgart, Baden-Württemberg, Germany.

Finley, A. O., and S. Banerjee (2013), *spBayes: Univariate and Multivariate Spatial-temporal Modeling*, R package version 0.3–6.

Finley, A. O., H. Sang, S. Banerjee, and A. E. Gelfand (2009), Improving the performance of predictive process modeling for large datasets, *Comput. Stat. Data Anal.*, *53*(8), 2873–2884, doi:10.1016/j.csda.2008.09.008.

Fuentes, M., and A. Raftery (2005), Model evaluation and spatial interpolation by Bayesian combination of observations with outputs from numerical models, *Biometrics*, *61*(1), 36–45.

Funk, C. C., P. J. Peterson, M. F. Landsfeld, D. H. Pedreros, J. P. Verdin, J. D. Rowland, B. E. Romero, G. J. Husak, J. C. Michaelsen, and A. P. Verdin (2014), A quasi-global precipitation time series for drought monitoring: U.S. Geological Survey Data Series 832, 4 pp. [Available at http://dx.doi.org/10.3133/ds832.]

Furrer, R., D. Nychka, and S. Sain (2012), *Fields: Tools for Spatial Data*, R package version 6.7.

Gallagher, K., K. Charvin, S. Nielsen, M. Sambridge, and J. Stephenson (2009), Markov chain Monte Carlo (MCMC) sampling methods to determine optimal models, model resolution and model choice for Earth Science problems, *Mar. Pet. Geol.*, *26*(4), 525–535, doi:10.1016/j.marpetgeo.2009.01.003.

Gorenburg, I. P., D. McLaughlin, and D. Entekhabi (2001), Scale-recursive assimilation of precipitation data, *Adv. Water Resour.*, *24*(2), 941–953.

Handcock, M., and M. Stein (1993), A Bayesian analysis of kriging, *Technometrics*, *35*(4), 403–410.

Huffman, G. J., R. F. Adler, B. Rudolf, U. Schneider, and P. R. Keehn (1995), Global precipitation estimates based on a technique for combining satellite-based estimates, rain gauge analysis, and NWP model precipitation information, *J. Clim.*, *8*, 1284–1295.

Huffman, G. J., R. F. Adler, P. Arkin, A. Chang, R. Ferraro, A. Gruber, J. Janowiak, A. Mcnab, B. Rudolf, and U. Schneider (1997), The Global Precipitation Climatology Project (GPCP) combined precipitation dataset, *Bull. Am. Meteorol. Soc.*, *78*(1), 5–20.

Huffman, G. J., R. F. Adler, M. M. Morrissey, D. T. Bolvin, S. Curtis, R. Joyce, B. McGavock, and J. Susskind (2001), Global precipitation at one-degree daily resolution from multisatellite observations, *J. Hydrometeorol.*, *2*, 36–50.

Huffman, G. J., D. T. Bolvin, E. J. Nelkin, D. B. Wolff, R. F. Adler, G. Gu, Y. Hong, K. P. Bowman, and E. F. Stocker (2007), The TRMM Multisatellite Precipitation Analysis (TMPA): Quasi-global, multiyear, combined-sensor precipitation estimates at fine scales, *J. Hydrometeorol.*, *8*(1), 38–55, doi:10.1175/JHM560.1.

Jin, B., Y. Wu, B. Miao, X. L. Wang, and P. Guo (2014), Bayesian spatiotemporal modeling for blending in situ observations with satellite precipitation estimates, *J. Geophys. Res. Atmos.*, *119*, 1806–1819, doi:10.1002/2013JD019648.

Joyce, R., and P. Arkin (1997), Improved estimates of tropical and subtropical precipitation using the GOES precipitation index, *J. Atmos. Oceanic Technol.*, *14*, 997–1011.

Joyce, R., J. Janowiak, P. Arkin, and P. Xie (2004), CMORPH: A method that produces global precipitation estimates from passive microwave and infrared data at high spatial and temporal resolution, *J. Hydrometeorol.*, *5*, 487–503.

Kidd, C., D. R. Kniveton, M. C. Todd, and T. J. Bellerby (2003), Satellite rainfall estimation using combined passive microwave and infrared algorithms, *J. Hydrometeorol.*, *4*, 1088–1104.

Kleiber, W., R. W. Katz, and B. Rajagopalan (2012), Daily spatiotemporal precipitation simulation using latent and transformed Gaussian processes, *Water Resour. Res.*, *48*, W01523, doi:10.1029/2011WR011105.

Kummerow, C., W. Barnes, T. Kozu, J. Shiue, and J. Simpson (1998), The Tropical Rainfall Measuring Mission (TRMM) sensor package, *J. Atmos. Oceanic Technol.*, *15*(3), 809–817, doi:10.1175/1520-0426(1998)015<0809:TTRMMT>2.0.CO;2.

Lawrimore, J. H., M. J. Menne, B. E. Gleason, C. N. Williams, D. B. Wuertz, R. S. Vose, and J. Rennie (2011), An overview of the Global Historical Climatology Network monthly mean temperature data set, version 3, *J. Geophys. Res.*, *116*, D19121, doi:10.1029/2011JD016187.

Le , N. D., and J. V. Zidek (1992), Interpolation with uncertain spatial covariances: A Bayesian alternative to kriging, *J. Multivariate Anal.*, *43*(2), 351–374, doi:10.1016/0047-259X(92)90040-M.

Le, N. D., and J. V. Zidek (2006), *Statistical Analysis of Environmental Space-Time Processes*, Springer, N. Y.

Lin, A., and X. L. Wang (2011), An algorithm for blending multiple satellite precipitation estimates with in situ precipitation measurements in Canada, *J. Geophys. Res.*, *116*, D21111, doi:10.1029/2011JD016359.

Metropolis, N., A. W. Rosenbluth, M. N. Rosenbluth, A. H. Teller, and E. Teller (1953), Equation of state calculations by fast computing machines, *J. Chem. Phys.*, *21*(6), 1087–1092, doi:10.1063/1.1699114.

Omre, H. (1987), Bayesian kriging—Merging observations and qualified guesses in kriging, *Math. Geol.*, *19*(1), 25–39.

Paciorek, C. (2010), The importance of scale for spatial-confounding bias and precision of spatial regression estimators, *Stat. Sci.*, *25*(1), 107–125.

R Development Core Team (2011), *R: A Language and Environment for Statistical Computing*, R Found. for Stat. Comput., Vienna. [Available at http://www.R-project.org/.]

Rozante, J. R., D. S. Moreira, L. G. G. de Goncalves, and D. A. Vila (2010), Combining TRMM and surface observations of precipitation: Technique and validation over South America, *Am. Meteorol. Soc.*, *25*, 885–894, doi:10.1175/2010WAF2222325.1.

Sahu, S. K., and K. V. Mardia (2005), A Bayesian kriged Kalman model for short-term forecasting of air pollution levels, *J. R. Stat. Soc., Ser. C*, *54*(1), 223–244, doi:10.1111/j.1467-9876.2005.00480.x.

Sansó, B., and L. Guenni (1999), Venezuelan rainfall data analysed by using a Bayesian spacetime model, *J. R. Stat. Soc., Ser. C*, *48*(3), 345–362, doi:10.1111/1467-9876.00157.

Sinclair, S., and G. Pegram (2005), Combining radar and rain gauge rainfall estimates using conditional merging, *Atmos. Sci. Lett.*, *6*(1), 19–22, doi:10.1002/asl.85.

Sorooshian, S., K.-L. Hsu, X. Gao, H. V. Gupta, B. Imam, and D. Braithwaite (2000), Evaluation of PERSIANN system satellite-based estimates of tropical rainfall, *Bull. Am. Meteorol. Soc.*, *81*(9), 2035–2046.

Tustison, B., E. Foufoula-Georgiou, and D. Harris (2002), Scale-recursive estimation for multisensor Quantitative Precipitation Forecast verification: A preliminary assessment, *J. Geophys. Res.*, *107*(D8), 8377, doi:10.1029/2001JD001073.

Verdin, A. (2013), Statistical methods for blending satellite and ground observations to improve high-resolution precipitation estimates, MS thesis, Univ. of Colo., Boulder, Colo.

Vila, D. A., L. G. G. de Goncalves, D. L. Toll, and J. R. Rozante (2009), Statistical evaluation of combined daily gauge observations and rainfall satellite estimates over continental South America, *J. Hydrometeorol.*, *10*, 533–543, doi:10.1175/2008JHM1048.1.

Xie, P., and P. Arkin (1997), Global precipitation: A 17-year monthly analysis based on gauge observations, satellite estimates, and numerical model outputs, *Bull. Am. Meteorol. Soc.*, *78*(11), 2539–2558.

Xie, P., and A.-Y. Xiong (2011), A conceptual model for constructing high-resolution gauge-satellite merged precipitation analyses, *J. Geophys. Res.*, *116*, D21106, doi:10.1029/2011JD016118.

Xie, P., J. E. Janowiak, P. A. Arkin, R. Adler, A. Gruber, R. Ferraro, G. J. Huffman, and S. Curtis (2003), GPCP pentad precipitation analyses: An experimental dataset based on gauge observations and satellite estimates, *J. Clim.*, *16*, 2197–2214.

Zhang, H. (2004), Inconsistent estimation and asymptotically equal interpolations in model-based geostatistics, *J. Am. Stat. Assoc.*, *99*(465), 250–261.